Melting spectral functions of the scalar and vector mesons in a holographic QCD model

Fujita, Mitsutoshi; Kikuchi, Toru

PHYSICAL REVIEW D **81,** 065024 (2010)

Melting spectral functions of the scalar and vector mesons in a holographic QCD model

Mitsutoshi Fujita* and Toru Kikuchi†
Department of Physics, Kyoto University, Kyoto 606-8502, Japan

Kenji Fukushima,‡ Tatsuhiro Misumi,§ and Masaki Murata‖
[1]*Yukawa Institute for Theoretical Physics, Kyoto University, Kyoto 606-8502, Japan*
(Received 20 November 2009; revised manuscript received 18 January 2010; published 22 March 2010)

We investigate the finite-temperature spectral functions of heavy quarkonia by using the soft-wall anti-de Sitter/QCD model. We discuss the scalar, the pseudoscalar, the vector, and the axial-vector mesons and compare their qualitative features of the melting temperature and growing width. We find that the axial-vector meson melts earlier than the vector meson, while there appears only a slight difference between the scalar and pseudoscalar mesons, which also melt earlier than the vector meson.

DOI: 10.1103/PhysRevD.81.065024 PACS numbers: 12.38.Mh, 11.25.Tq, 14.40.−n, 25.75.Nq

I. INTRODUCTION

The strongly correlated quark-gluon plasma (sQGP), which is hot and dense matter out of quarks and gluons created at the Relativistic Heavy-Ion Collider in the Brookhaven National Laboratory, have been attracting a great deal of interest in its intrinsic nonperturbative properties [1–3]. Although there is no systematic way to study such a nonperturbative system at strong coupling, a powerful technique has developed recently based on the gauge/string correspondence [4–6]. The idea is that one can treat the strong-coupling regime in the gauge field theory on the boundary by solving the weak-coupling string theory (or classical one in the large N_c and large 't Hooft coupling limit) in the bulk anti de Sitter (AdS) space.

A well-known example of successful application of the gauge/string duality to the sQGP physics is the exact computation of the shear viscosity to the entropy density ratio, i.e. $\eta/s = \hbar/(4\pi k_B)$ in an $\mathcal{N} = 4$ supersymmetric Yang-Mills plasma [7–10]. This value of η/s is much smaller than any observation in reality except for the heavy-ion collisions; the hydrodynamic model studies imply that η/s of QCD matter is as small as suggested by the string theory [11,12]. Besides, it is conjectured that $\eta/s = \hbar/(4\pi k_B)$ might be a universal lower bound and applied to strong-coupling QCD as well as supersymmetric models.

The smallness of η/s is an important indication of the sQGP because a larger reaction cross section leads to a smaller η in gaseous states. Actually, perturbative QCD calculations cannot give account for small η/s in the weak-coupling regime [13–15]. The Monte Carlo simulation of QCD on the lattice is a powerful instrument to look into the nonperturbative strong-coupling regime. It is still difficult to estimate η in fully dynamical simulations with quarks, but the (quenched) results so far are not inconsistent with the string theory estimate [16,17].

Another important indication to the sQGP is the in-medium property of heavy quarkonia such as J/ψ. In the recent lattice QCD simulations the J/ψ spectral functions (SPFs) both above and below T_c have been successfully constructed by means of the maximum entropy method [18], which has indicated that the mesonic correlation (a peak in the SPF) survives even above twice that of T_c [19–23]. It is, however, a nontrivial question how to explain such a high melting temperature for J/ψ in a conventional way using the nonrelativistic model with the Debye screened potential [24–28]. We have not yet reached a full consensus on the interpretation of the J/ψ SPFs above T_c, though there are many theoretical efforts. Our present aim is to investigate this question using the gauge/string duality along the same line as our previous work [29].

In Ref. [29] we calculated the SPFs in the vector channel assuming that the heavy-quark sector is decoupled from others. In this work we will extend our analysis to other channels; scalar, pseudoscalar, and axial-vector mesons, namely, χ_{c0}, η_c, and χ_{c1}. Since the interpretation of χ_{c0} (i.e. whether it melts or not above T_c) was controversial [21–23], it is important to clarify whether $c\bar{c}$ states in all these channels melt at $T > T_c$ and, if so, when they melt. Under the situation that the maximum entropy method construction of the SPFs in lattice QCD simulations are still difficult for all these channels, it is valuable to take advantage of the holographic QCD model to see what spectral shape would transpire in the strongly coupling system. In this work we will use the soft-wall AdS/QCD model [30,31] (see Refs. [32,33] for related works). Although the SPFs at finite temperature and density have been discussed by means of the D3/D7 setup [34], it is not straightforward to deal with the heavy-meson SPFs in the D3/D7 model. This is because the only energy scale in this model is fixed by the pion decay constant and the SPFs are given as a function of not T and M_q independently but only T/M_q where M_q is the quark mass [35,36]. The soft-wall

*mfujita@gauge.scphys.kyoto-u.ac.jp
†kikuchi@gauge.scphys.kyoto-u.ac.jp
‡fuku@yukawa.kyoto-u.ac.jp
§misumi@yukawa.kyoto-u.ac.jp
‖masaki@yukawa.kyoto-u.ac.jp

model, in contrast, has one more phenomenological parameter, c, which is fixed by the meson spectrum.

One of the important features in the soft-wall AdS/QCD model is that a parameter in the bifundamental scalar sector controls the chiral symmetry breaking, that is, the chiral condensate. Interestingly enough, the chiral condensate is uniquely determined from the infrared (IR) boundary condition that is specified by a smooth function in the soft-wall model. Therefore, in this model, there is no ambiguity in the IR limit in the case at finite T (see Refs. [37,38] for holographic approaches to finite-T mesons). The regular IR boundary condition allows us to evaluate the Minkowskian correlator [39–41] from which we can compute the SPFs. We will find, in view of the resultant SPFs, that the axial-vector states melt faster than the vector ones. We will then clarify its origin in the chiral symmetry breaking due to the scalar field which yields a difference between the vector and axial-vector equations of motion. On the other hand, the scalar and pseudoscalar dissociation temperatures are almost the same; $T \simeq T_c$. Finally, before closing this paper, we shall take a closer look at the vector channel.

II. SOFT-WALL MODEL

The principle to construct the AdS/QCD model is the bulk/boundary correspondence or UV/IR relation. The generating functional in the gauge field theory is equivalent to the exponential of an on-shell action in the gravity theory (Gubser-Klebanov-Polyakov-Witten relation [5,6]),

$$Z[\phi_0] = \langle e^{i\int dx \phi_0(x)\mathcal{O}(x)}\rangle_{\text{gauge}} = e^{iS_{\text{gravity}}[\phi_0]}, \tag{1}$$

where $Z[\phi_0]$ is the generating functional with the source ϕ_0 coupled with an operator $\mathcal{O}(x)$ and S_{gravity} is an on-shell action with the boundary condition $\phi \to \phi_0$ at the UV boundary where the gauge theory resides.

The AdS/QCD models are five-dimensional field theories designed to describe QCD properties through the bulk/boundary correspondence [32]. The essential ingredients of the AdS/QCD model are the AdS space with an IR cutoff (i.e. wall) that translates into a typical energy scale in QCD, the $\mathrm{U}_L(2) \times \mathrm{U}_R(2)$ vector fields, A_L, A_R, and the bifundamental scalar field X. The vacuum expectation value of X is responsible for the explicit and spontaneous chiral symmetry breaking. The soft-wall model is defined by the following action [31]:

$$S = \int d^5x e^{-c_\rho z^2}\sqrt{-g}\,\mathcal{L}, \tag{2}$$

$$\mathcal{L} = \mathrm{tr}\Big[-|DX|^2 + \frac{3}{L^2}|X|^2 - \frac{1}{4g_5^2}(g^{MN}g^{PQ}F_{L,MP}F_{L,NQ} + g^{MN}g^{PQ}F_{R,MP}F_{R,NQ})\Big], \tag{3}$$

where $X = X^a t^a$ with t^a being the generator of $U(2)$ and $D_M X = \partial_M X + iA_{L,M}X - iXA_{R,M}$. Here, $M = x_0, x_1, x_2, x_3, z$ and g_5 are the indices for the five-dimensional coordinates and gauge coupling, respectively. We note that $g_5^2 = 24\pi^2 L/N_c$ is concluded by matching [31]. We also use the Greek index $\mu = x_0, x_1, x_2, x_3$ to refer to the four-dimensional coordinates. The model parameter, c_ρ, characterizes the wall location; since the contribution from the IR region $z \gtrsim 1/\sqrt{c_\rho}$ is suppressed by $e^{-c_\rho z^2}$, it represents a potential with the wall providing a typical QCD scale. The background geometry is specified as the AdS metric as

$$g_{MN}dx^M dx^N = \frac{L^2}{z^2}(-dt^2 + d\vec{x}^2 + dz^2). \tag{4}$$

It should be mentioned that the vector-meson mass spectra at $T = 0$ are quantized by the normalizability condition and given as the following Regge trajectory: [31],

$$m_n^2 = 4c_\rho n, \tag{5}$$

where n is the radial excitation number. Then we can determine c_ρ by fitting the above relation to the vector-meson spectra; $\rho(770)$, $\rho(1450)$, $\rho(1700)$, etc. If we take $m_\rho = 0.77$ GeV for $n = 1$, we have $c_\rho = 0.77^2/4 = 0.148$ GeV^2, while we will later find that the spectral peak is slightly shifted from Eq. (5) and will fix $c_\rho = 0.151$ GeV^2 to fit the peak position with the mass.

Now that we fix the model parameter c_ρ, let us consider the model at finite temperature. Here, we shall introduce the following background, which is called the AdS black-hole (AdSBH),

$$g_{MN}dx^M dx^N = \frac{L^2}{z^2}\left(-f(z)dt^2 + d\vec{x}^2 + \frac{1}{f(z)}dz^2\right), \tag{6}$$

with $f(z) = 1 - z^4/z_h^4$ where the horizon is related to the Hawking temperature that is interpreted as the system temperature of dual QCD as $z_h = 1/(\pi T)$. It is known that the AdSBH is unstable at low temperature, and thus the Hawking-Page-type transition occurs at a critical temperature, $T_c = 0.492\sqrt{c_\rho}$. This is a first-order phase transition from the AdSBH to the thermal AdS metric [42,43] as the temperature is lowered and is a phase transition from the deconfined to the confined phase.

In the soft-wall model one can introduce the chiral symmetry breaking explicitly (i.e. quark mass) and spontaneously (i.e. chiral condensate) through the bifundamental scalar field X, which is decomposed as $X(x,z) = e^{2i\Pi(x,z)}[X_0(z) + S(x,z)]$ where x refers to four-dimensional coordinates only and X_0 is a constant background with respect to x. The fluctuations, S and Π, represent the scalar and pseudoscalar fields. In the case when quark masses are degenerated, $X_0(z)$ is proportional to unity in flavor space and satisfies the following equation of motion:

$$X_0''(z) + \left(-2cz + \frac{f-4}{zf}\right)X_0'(z) + \frac{3}{z^2 f}X_0(z) = 0, \quad (7)$$

where the prime stands for the derivative with respect to z. From this differential equation we find that in the vicinity of $z = 0$ the general solution behaves as

$$L^{3/2}X_0(z) \sim \tfrac{1}{2}(M_q z + \Sigma z^3), \quad (8)$$

where, according to the dictionary of bulk/boundary correspondence, the parameters M_q and Σ are identified with the quark mass matrix and the chiral condensate, respectively. Here, in the soft-wall model, Σ is uniquely determined for a given M_q so that Eq. (7) can yield a finite and regular solution of X_0. This property is a flaw in the light-quark sector because $M_q = 0$ always leads to $\Sigma = 0$ and so the spontaneous breaking of chiral symmetry is not correctly described unless Eq. (7) is modified with higher-order potential terms [44,45]. In the present work, as we discuss later, only the heavy-quark sector is of interest to us, and we need not alter Eq. (7) because chiral symmetry is largely broken in an explicit manner.

We must point out that the conventional soft-wall model has another flaw in the chiral properties. In the vicinity of the UV limit two independent solutions of Eq. (7) are definitely z and z^3, but if we carefully go beyond the leading order, the former solution receives a correction by a logarithmic term as $z \to z + (-1/2 + \log z)z^3$. This higher-order correction is small as compared to z, but not small at all to another solution z^3. Therefore, Eq. (7) leads to a UV divergent chiral condensate, which is an artifact of the soft-wall model. (There is no such logarithmic term in the hard-wall model.) Therefore, we need to modify the model as done in Refs. [44,45], for example. In the present work we will take the following strategy. That is, to solve Eq. (7) numerically, we will force the initial condition by Eq. (8) and find Σ in such a way that the solution in the IR region contains no singularity. This is not a fully satisfactory resolution but is acceptable pragmatically for the soft-wall model that is only a phenomenological model.

Let us mention on the asymptotic solutions of X_0 near the horizon ($z \simeq z_h$) for the finite-T case. Equation (7) can simplify by the variable change from z to $t = \sqrt{3(1 - z/z_h)}$, which reduces to the Bessel equation near the horizon $t \sim 0$. It is thus obvious that the asymptotic solutions of X_0 are given by the first-kind Bessel function $J_0(t)$ which is regular and the second-kind Bessel function $Y_0(t)$ which is divergent at $t = 0$. Since the physical solution must yield a finite action, we should pick only $J_0(t)$ up near $z = z_h$. To this end we need adjust an appropriate ratio of M_q and Σ in the initial condition (8) in the UV boundary, so that it evolves to $J_0(t)$ near the horizon. We will concretely carry this procedure out in later discussions.

III. FLAVOR-DEPENDENT SOFT-WALL MODEL

The mass spectra (5) in the soft-wall model successfully reproduce the Regge trajectory of the light vector mesons consisting of u and d quarks as seen in the previous section. In order to apply this model description to the heavy-quark sector, we propose a modification on the soft-wall model in such a way that we treat c as a flavor-dependent parameter. The following action in our treatment is composed from two sectors: one is the light-quark (u, d, s) sector and the other is the heavy-quark (c) sector,

$$S = \int d^5x\sqrt{-g}\,\mathrm{tr}(e^{-c_\rho z^2}\mathcal{L}_{\mathrm{light}} + e^{-c_{J/\psi}z^2}\mathcal{L}_{\mathrm{heavy}}), \quad (9)$$

where $\mathcal{L}_{\mathrm{heavy}}$ takes an almost identical structure with Eq. (3) in the light-quark sector. The only difference is that fields in $\mathcal{L}_{\mathrm{light}}$ and in $\mathcal{L}_{\mathrm{heavy}}$ belong to U(3) and U(1) groups, respectively. From the vector-meson mass formula (5), we can determine the model parameters as

$$c_\rho = 0.151\ \mathrm{GeV}^2, \qquad c_{J/\Psi} = 2.43\ \mathrm{GeV}^2, \quad (10)$$

to reproduce $m_\rho = 0.77$ GeV and $m_{J/\psi} = 3.1$ GeV (as we have noted, the spectral peak is slightly different from Eq. (5) and c is shifted from the naive estimates accordingly). If we believe in the mass formula, the above value of $c_{J/\psi}$ predicts the mass of the first excited state as 4.4 GeV, which overestimates the mass of $\psi(2S)$ that is 3.7 GeV. Therefore, this deviation by around 20% should be taken for a systematic error in this model [38]. We note that the holographic model is not very successful to reproduce the charmonium mass spectrum in the vacuum. This is a caveat in our present work. Our analysis here should be thus limited only to the qualitative investigation of in-medium effects on the SPF behavior. To this and only this end it is meaningful to utilize the holographic approach.

Because of $c_\rho \ll c_{J/\psi}$, the latter term in the action (9) is negligible to evaluate the magnitude of S. Hence, the critical temperature T_c of the Hawking-Page transition in this model is solely determined by the former term involving c_ρ, that means $T_c = 0.492\sqrt{c_\rho} = 0.191$ GeV is unchanged. In short, the bulk thermodynamics is dominated by the former term, while the heavy-flavor sector is described by the equation of motion deduced from the latter term the action (9).

Before closing this section let us comment on possible justification of this model treatment with two scales. One may wonder that c should be common to all flavors because it is a parameter related to the QCD string tension. Besides, it should be more natural that $m_{J/\psi}$ arises mostly from M_q rather than $c_{J/\psi}$. In the soft-wall model, however, the vector-meson field has no direct coupling with X_0 and so it does not depend on M_q. The important point is that $c_{J/\psi}$ as a "renormalized" scale can originate from the back-reaction with the heavy charm-quark mass beyond

the probe approximation. In fact it is pointed out in Ref. [44] that the backreaction from the X field in the hard-wall model produces an effective soft wall with c depending on M_q. So far there is no such analysis on the backreaction within the framework of the soft-wall model, but it would be a reasonable anticipation that c must get larger with heavier M_q once the back-reaction is taken into account. The backreaction analysis in the top-down approaches [46,47] also implies that our treatment could be pragmatically acceptable. In the next section we simply denote $c_{J/\psi}$ as c.

IV. SPECTRAL FUNCTIONS

In this section we proceed to actual calculation of the SPFs. As seen from the bulk/boundary correspondence, we can derive the SPFs in the channel of our interest by solving the classical equation of motion in five dimensions. Here, we take the AdS radius as $L = 1$ since this quantity disappears in the physical correlation functions. In addition, for convenience, we use the dimensionless energy ω, momentum q, and temperature t in the unit of $\sqrt{c} = \sqrt{c_{J/\psi}}$ and change the variable for the fifth coordinate by $\xi = \sqrt{c_{J/\psi}}z = \sqrt{c}z$, so that we can totally eliminate c from the equation of motion. Because only c is a dimensional parameter in the model, we can easily restore c to discuss physical quantities. It should be noted that spatial and temporal components lead to distinct differential equations since Lorentz symmetry is broken in the presence of a medium. For the moment we will focus on the solution of spatial fields in this section, then in Sec. V C we will address a physics insight into the dependence on the polarization direction.

Here, we make an important remark on the interpretation of our results shown in what follows below. Strictly speaking, the SPFs obtained by means of the AdSBH background make sense only for $t > T_c/\sqrt{c_{J/\psi}} = 0.492\sqrt{c_\rho/c_{J/\psi}} = 0.122$ where the AdSBH metric is more favored. We must say, therefore, that all the SPF curves for $t < 0.122$ are not physical ones, which is an obvious deficiency in our treatment. If a spectral peak widens and disappears far below $t = 0.122$ as is the case for the axial-vector channel, what should really happen in the SPFs is that a sharp peak is not changed at all up to $t = 0.122$ and then a first-order Hawking-Page transition lets it melt away completely. The reasons why we still like to show results at $t < 0.122$ are as follows; First, the critical value of t may not be 0.122 or may be smaller because the soft-wall model is defined in such a way that the metric does not solve the gravity equation. This problem would be clarified in a more consistent model beyond the soft-wall implementation. Second, what we are interested in is not the large-N_c world but the real QCD world in which the finite-T transition is smooth crossover. Since there is no sharp transition in QCD, it is conceivable to expect that the extrapolation from above to below T_c may be useful as a plausible guess about the situation around the crossover region in QCD.

A. Vector mesons

Let us first consider the vector meson whose dual field is $V_M = (A_{L,M} + A_{R,M})/2$ and then the axial-vector meson whose dual field is $A_M = (A_{L,M} - A_{R,M})/2$. We fix the gauge by choosing $A_{L,z} = A_{R,z} = 0$. Besides, we impose $\partial^\mu A_{L,\mu} = \partial^\mu A_{R,\mu} = 0$ to get rid of unphysical polarization. The linearized equation of motion for the spatial component V_x (either $x = x_1$, x_2, or x_3) of the vector field takes the following form:

$$\partial_z[e^{-cz^2}\sqrt{-g}g^{xx}g^{zz}(\partial_z V_x)] + [e^{-cz^2}\sqrt{-g}g^{xx}\partial_\mu\partial^\mu V_x] = 0. \tag{11}$$

Now we move to momentum space by performing the Fourier transformation, $V_x(x, \xi) = \int d^4x e^{i\sqrt{c}p\cdot x}\tilde{V}(p)v(\xi; p)$ and substitute the AdSBH metric (6) into Eq. (11), so that we reach,

$$v'' + \left(\frac{3f-4}{\xi f} - 2\xi\right)v' + \left(\frac{\omega^2}{f^2} - \frac{q^2}{f}\right)v = 0, \tag{12}$$

with $p^\mu = (\omega, q^1, q^2, q^3)$ and $q^2 = (q^1)^2 + (q^2)^2 + (q^3)^2$. Here, as we have mentioned before, all variables are dimensionless and the prime ($'$) stands for the derivative with respect to ξ.

Before solving Eq. (12) it would be instructive to pursue the analogy to the Schrödinger equation in quantum mechanics. The change of the field, $u = (e^{-cz^2}\sqrt{-g}g^{xx}g^{zz})^{1/2}v$, simplifies the equation of motion in the following form: $u'' - U_v(\xi)u = 0$, with the potential

$$U_v(\xi) = \xi^2 + \frac{3}{4\xi^2} - \frac{f'}{f}\left(2\xi + \frac{1}{\xi}\right) - \frac{(f')^2}{4f^2} + \frac{f''}{2f} - \frac{1}{f}\left(\frac{\omega^2}{f} - q^2\right). \tag{13}$$

Figure 1 shows this potential for various dimensionless temperatures in the unit of $\sqrt{c}$. In the case at $T = 0$ (and thus $f = 1$) the downward-convex potential, $\xi^2 + 3/(4\xi^2)$, yields the discrete spectrum, $m^2 = \omega^2 - q^2 = 4n$ ($n = 1, 2, \ldots$), only for which the wave function is normalizable. We see that the higher t or smaller $\xi_h = 1/(\pi t)$ makes the potential less convex and eventually it becomes monotonic at $t \simeq 0.15$. With a monotonic potential we cannot expect a remnant of the original spectrum any longer. In other words we should anticipate dissociation then. Let us confirm this in what follows.

At finite temperature the potential is no longer rising in the large z side and the normalizability does not quantize the spectrum. We can easily extract the asymptotic solutions of Eq. (12) near the horizon as

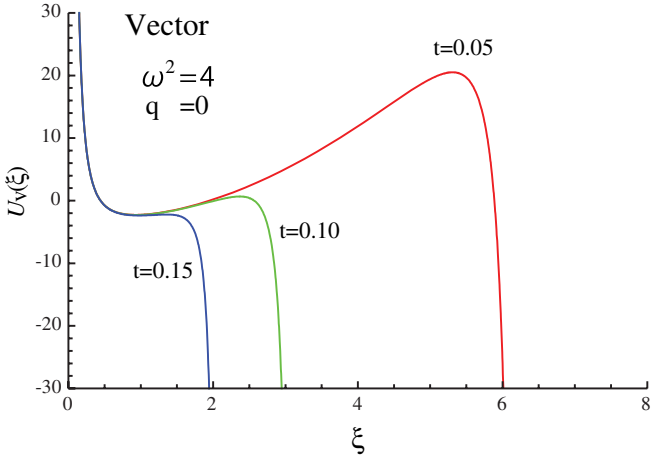

FIG. 1 (color online). Potential $U_v(\xi)$ for the vector fields at dimensionless temperatures, $t = T/\sqrt{c} = 0.05$, 0.10, and 0.15 at $\omega^2 = 4$ and $q^2 = 0$. $\xi = \sqrt{c}z$, $t = T/\sqrt{c}$, and ω and q are given in the unit of $\sqrt{c}$.

$$v(\xi) \to c_+\phi_+ + c_-\phi_- \quad \text{with} \quad \phi_\pm = (1 - \xi/\xi_h)^{\pm i\omega\xi_h/4}, \tag{14}$$

in the vicinity of $\xi \to \xi_h$. Here, ϕ_+ represents the outcoming solution and ϕ_- the in-falling solution into the black hole. Near the origin, on the other hand, the solution has the following asymptotic form:

$$v(\xi) = A\Phi_1 + B\Phi_0, \tag{15}$$

where Φ_1 and Φ_0 are two solutions of Eq. (11) satisfying the following UV boundary conditions:

$$\Phi_1 \to -\frac{\pi}{2}\sqrt{\omega^2 - q^2}\,\xi Y_1(\sqrt{\omega^2 - q^2}\,\xi), \quad \Phi_0 \to \frac{2}{\sqrt{\omega^2 - q^2}}\,\xi J_1(\sqrt{\omega^2 - q^2}\,\xi), \tag{16}$$

around $\xi \to 0$. Here, J_1 and Y_1 are the first-kind and second-kind Bessel functions, respectively. In the above we normalized Φ_1 and Φ_0 in such a way that $\Phi_1(\xi = \epsilon) = 1$ and $\Phi_0(\xi = \epsilon) = \epsilon^2$ and also we assumed that $\omega^2 > q^2$. In the case that $q^2 > \omega^2$ we should replace the above by $\Phi_1 \to \sqrt{q^2 - \omega^2}\,\xi K_1(\sqrt{\omega^2 - q^2}\,\xi)$ and $\Phi_0 \to (2/\sqrt{q^2 - \omega^2})\,\xi I_1(\sqrt{\omega^2 - q^2}\,\xi)$. In what follows we will fix the overall normalization of $v(\xi)$ by adopting the commonly used prescription, $A = 1$, so that B should be unique once the IR boundary condition is specified.

Following the procedure elucidated in great details in Refs. [39–41] we can compute the Green's function in Minkowskian space-time. The IR boundary condition must be $v(\xi \to \xi_h) = c_-\phi_-$ (i.e. $c_+ = 0$) to acquire the retarded Green's function according to Ref. [39]. We can make $v(\xi)$ satisfy this IR boundary condition by choosing B appropriately at $\xi \simeq 0$ (where $A = 1$ is chosen so that $v(\xi \to \epsilon) = 1$); Then, B, which is now a complex number, is uniquely fixed by the IR boundary condition:

$$v(\xi) = \Phi_1(\xi) + B(\omega, q)\Phi_0(\xi) \to c_-\phi_-(\xi) \quad \text{as } \xi \to \xi_h. \tag{17}$$

As we defined above, we can generally solve Φ_1 and Φ_0 from Eq. (11) from the UV asymptotic forms (16) toward the IR side. If we have,

$$\Phi_i(\xi) \to a_i(\omega, q)\phi_+(\xi) + b_i(\omega, q)\phi_-(\xi), \tag{18}$$

where $i = 0$, 1, then we can readily conclude $B(\omega, q) = -a_1/a_0$.

Once B is obtained, the bulk/boundary correspondence (1) allows us to compute the Green's function, that is given as

$$D^R(\omega, q) = -C\lim_{\xi\to\epsilon}\left(\frac{1}{\xi}v^*v'\right) = -2C\left[B(\omega, q) - \frac{\omega^2 - q^2}{2} \times \ln\left(\frac{e^{\gamma_E}}{2}\sqrt{|\omega^2 - q^2|}\,\epsilon\right)\right], \tag{19}$$

where C is a constant given as $C = N_c^2/(64\pi^2 L)$. The spectral function is, by its definition,

$$\rho(\omega, q) = -\frac{1}{\pi}\,\mathrm{Im}D^R(\omega, q) = \frac{2C}{\pi}\,\mathrm{Im}B(\omega, q). \tag{20}$$

Here, we note that only $B(\omega, q)$ has an imaginary part in Eq. (19).

We are now ready to come to the numerical calculation. We plot $\mathrm{Im}B(\omega, q)$ by calculating $a_i(\omega, q)$ numerically as a function of ω and q at various temperatures and show the SPFs at $q = 0$ in Fig. 2. We should remark our convention that we refer to $\mathrm{Im}B(\omega, q)$ as the SPF neglecting an overall factor.

B. Axial-vector mesons

Next we shall move to the SPFs in the axial-vector channel. We can follow exactly the same procedure as the previous one to look into the axial-vector fields, which we denote as $A_M = (A_{L,M} - A_{R,M})/2$. We again define the Fourier mode of the transverse component A_x (where either $x = x_1$, x_2, or x_3), i.e. $a(\xi; p)$. The dimensionless equation of motion is expressed as

$$a''(\xi) + \left(\frac{3f - 4}{\xi f} - 2\xi\right)a'(\xi) + \left(\frac{\omega^2}{f^2} - \frac{q^2}{f}\right)a(\xi) + \frac{96\pi^2}{N_c\xi^2 f}X_0^2 a(\xi) = 0. \tag{21}$$

We see that the above (21) is just the same as Eq. (11) for the vector fields except for the last term involving X_0^2 where X_0 is a solution of Eq. (7). The chiral symmetry breaking from $M_q \neq 0$ and $\Sigma \neq 0$ is introduced by $X_0 \sim \frac{1}{2}(M_q\xi + \Sigma\xi^3)$ near $\xi = 0$ and is responsible for the mass splitting

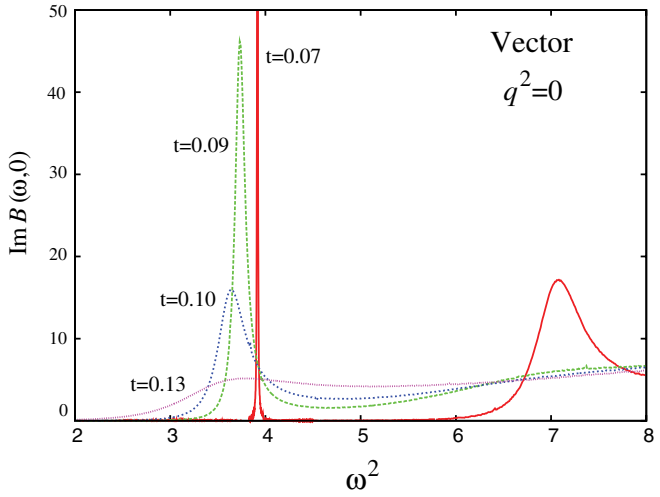

FIG. 2 (color online). Vector spectral functions $\mathrm{Im}B(\omega, 0)$ for the temperatures, $t = 0.07$, 0.09, 0.10, and 0.13. The melting temperature for the lowest-lying peak is about $t = 0.14$. $t = T/\sqrt{c}$, and ω and q are given in the unit of $\sqrt{c}$.

between the vector and axial-vector channels. We can also expect the last term becomes negligible as compared to the third term for large ω or q, so that the highly excited radial states exhibit degeneracy between the vector and axial-vector mesons [45], which has been observed in the excited baryon spectrum [48]. As discussed in Sec. II, the quark mass M_q and the chiral condensate Σ are not independent in the soft-wall model and once M_q is fixed, Σ is uniquely determined so as to yield a regular solution of X_0 in the IR region under a requirement that the UV initial condition is forced to be Eq. (8).

Now we fix M_q as the charm mass,

$$M_q = M_{\mathrm{charm}} = 1.30\ \mathrm{GeV}, \tag{22}$$

to derive the associated chiral condensate Σ by the shooting method numerically. In our calculation we obtain $\Sigma \simeq -(3.1\ \mathrm{GeV})^3$, which seems overestimation but within a reasonable range of order. Using these M_q and Σ we can get a regular numerical solution of the background scalar field $X_0(\xi)$. One noticeable fact to be mentioned is that, since X_0 is regular for an appropriate choice of M_q and Σ both near the horizon $\xi \sim \xi_h$ and near the boundary $\xi = 0$, the boundary conditions for $a(\xi)$ are (almost) the same as those for $v(\xi)$ as follows:

$$a(\xi) \to c_+\phi_+ + c_-\phi_-, \tag{23}$$

near $\xi \to \xi_h$, and near the UV boundary we have

$$a(\xi) = A\Phi_1' + B\Phi_0', \tag{24}$$

where Φ_1' and Φ_0' are two solutions of Eq. (21) satisfying Eq. (16) with $\omega^2 - q^2$ replaced by $\omega^2 - q^2 + (24\pi^2/N_c)M_q^2$.

Hereafter we will trace the same analysis from Eq. (13) to Eq. (20) in the previous subsection. In the picture of the Schrödinger equation the corresponding potential for the axial-vector case is given by

$$U_a(\xi) = \xi^2 + \frac{3}{4\xi^2} - \frac{f'}{f}\left(2\xi + \frac{1}{\xi}\right) - \frac{(f')^2}{4f^2} + \frac{f''}{2f} - \frac{1}{f}\left(\frac{\omega^2}{f} - q^2\right) + \frac{96\pi^2}{N_c\xi^2 f}X_0^2. \tag{25}$$

We show the profile of $U_a(\xi)$ in Fig. 3. It is clear in view of Figs. 1 and 3 that the axial-vector potential becomes less downward-convex earlier than the vector case, and the shape looks monotonic already around $t \simeq 0.10$. Thus, we can anticipate that the axial-vector spectral peaks should melt much earlier than the vector ones. In fact, $t \simeq 0.10$ corresponds to $T = 0.10\sqrt{c} = 0.16$ GeV, which is below the deconfinement temperature $T_c = 0.191$ GeV, meaning that the axial-vector mesons should melt at the phase transition.

Now let us derive the axial-vector SPFs. The solution satisfying the in-falling boundary condition determines a complex value of $B(\omega, q)$,

$$a(\xi) = \Phi_1'(\xi) + B(\omega, q)\Phi_0'(\xi) \to c_-\phi_-(\xi) \quad \text{as } \xi \to \xi_h. \tag{26}$$

Through the same procedure as elaborated in the previous subsection, we estimate the SPFs for the axial-vector mesons by evaluating $\mathrm{Im}B(\omega, q)$ numerically. We show our numerical results for the axial-vector SPFs with $q = 0$ in Fig. 4. Here, we depict $\mathrm{Im}B(\omega, q)$ divided by 10 to make its scale similar to Fig. 2. The overall factor takes a different value depending on the vector and axial-vector channels because of our normalization convention $A = 1$. Therefore, under the choice of $A = 1$, it is not a physically

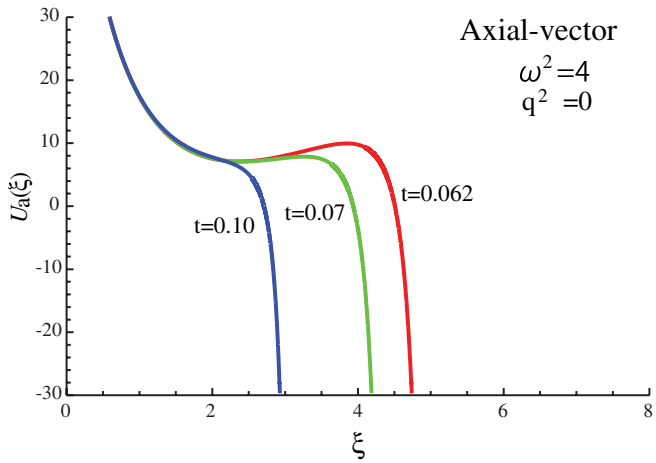

FIG. 3 (color online). Potential $U_a(\xi)$ for the axial-vector fields at dimensionless temperatures, $t = 0.062$, 0.07, and 0.10 at $\omega^2 = 4$ and $q^2 = 0$. $\xi = \sqrt{c}z$, $t = T/\sqrt{c}$, and ω and q are given in the unit of $\sqrt{c}$.

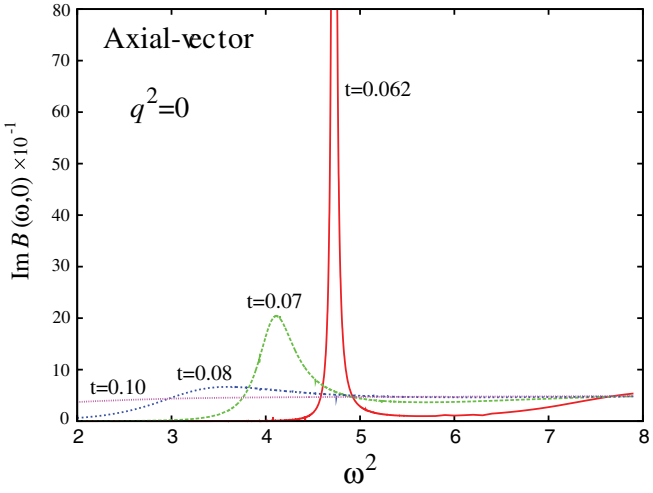

FIG. 4 (color online). Axial-vector spectral functions $\mathrm{Im}B(\omega,0)\times10^{-1}$ for the temperatures, $t=0.062$, 0.07, 0.08, and 0.10. The melting temperature for the lowest-lying peak is about $t\simeq0.10$. $t=T/\sqrt{c}$, and ω and q are given in the unit of $\sqrt{c}$.

meaningful comparison to take the absolute magnitude of spectral heights seriously.

C. Discussions for vector and axial-vector mesons

Here, let us make a comparison between the vector (Fig. 2) and axial-vector (Fig. 4) channels. For low temperatures, the lowest-lying peaks are located at $\omega^2=3.92$ for the vector case and $\omega^2=4.72$ for the axial-vector case. If we fix $c=2.43$ GeV^2 to reproduce $m_{J/\psi}=3.1$ GeV, then we have the mass in the axial-vector channel as $m_{\chi_{c1}}=3.4$ GeV, that is in agreement with the experimental value 3.51 GeV.

It is an apparent feature seen in Figs. 2 and 4 that the spectral peaks become more collapsed, and the peak positions move smaller as t increases. We also note that the second lowest-lying states melt far earlier than the lowest-lying states both in the vector and axial-vector cases. This is quite natural because higher excited states are less stable generally. In terms of the potentials illustrated in Figs. 1 and 3 a larger ω^2 causes stronger absorption into the black hole by the term, $-\omega^2/f^2$, which is negative large near the horizon. Furthermore, as seen from the $t=0.07$ curve in Fig. 2, the lowest-lying state moves smaller only slightly, while the excited states shift more drastically. These qualitative properties of the SPFs are consistent with the lattice QCD observations for the heavy quarkonia.

As seen from Figs. 2 and 4, the dissociation takes place around $T\simeq0.15\sqrt{c}\simeq0.23$ GeV for the vector lowest-lying peak and around $T\simeq0.10\sqrt{c}\simeq0.16$ GeV for the axial-vector one, where $c=c_{J/\psi}=2.43$ GeV^2 as discussed before. The deconfinement transition occurs at $T_c=0.492\sqrt{c}=0.19$ GeV as mentioned in Sec. III. Thus, in our soft-wall QCD model, the vector charmonium J/ψ melts above the critical temperature; $T\simeq1.2T_c$, while the dissociation temperature of the axial-vector charmonium χ_{c1} is much lower; $T\simeq0.8T_c$, which indicates that χ_{c1} does not survive above T_c and melts suddenly at the deconfinement transition. It is obvious in our argument that the chiral symmetry breaking induced by X_0 causes this difference between the vector and axial-vector SPFs.

D. Scalar and pseudoscalar mesons

Here, we go on to the SPF for the scalar and pseudoscalar fields, whose lowest-lying peak can be identified as χ_{c0} and η_{c0}. As discussed in Sec. II, we can introduce the dual fields of the scalar and pseudoscalar mesons by decomposing the bifundamental scalar field as $X=e^{2i\Pi(x,z)}[X_0(z)+S(x,z)]$, where X_0 is the background part, S is the scalar field and Π the pseudoscalar field. We will denote the Fourier modes of S and Π as s and π, respectively, in what follows below.

Before addressing the SPFs, we need to consider the holographic renormalization and counter terms [49–51] to give regular results near the boundary as well as physically meaningful SPFs in the scalar channel. The action with respect to the scalar and pseudoscalar fields in the quadratic order of S^2 and Π^2 is given by

$$S=\int_{z=0}d^4x\frac{e^{-cz^2}}{z^3}(-S'S-4X_0^2\Pi'\Pi)+S_{\mathrm{eom}} \tag{27}$$

after the integration by parts, in which the functional derivative of S_{eom} leads to the equations of motion. The first term is UV divergent at $z\to0$ and requires the renormalization counter term that is constructed in such a way that the covariance holds;

$$S_{\mathrm{ren}}=\int_{z=0}d^4xe^{-cz^2}\sqrt{-\gamma}X^2, \tag{28}$$

where γ is the determinant of the induced metric defined as $\gamma_{\mu\nu}=\mathrm{diag}(-fz^{-2},z^{-2},z^{-2},z^{-2})$ and thus $\sqrt{-\gamma}\sim z^{-4}$ near $z=0$. The renormalized action is defined as $S+S_{\mathrm{ren}}$ [49–51]. Once we comply with this renormalized procedure, we can follow the same procedure as in the previous case for the vector and axial-vector mesons. In this way we find the dimensionless equation of motion for the scalar and pseudoscalar fields;

$$s''(\xi)+\left(\frac{f-4}{\xi f}-2\xi\right)s'(\xi)+\left(\frac{\omega^2}{f^2}-\frac{q^2}{f}+\frac{3}{\xi^2f}\right)s(\xi)=0, \tag{29}$$

$$\pi''(\xi)+\left(\frac{f-4}{\xi f}-2\xi+\frac{2X_0'}{X_0}\right)\pi'(\xi)+\left(\frac{\omega^2}{f^2}-\frac{q^2}{f}\right)\pi(\xi)=0. \tag{30}$$

Here, the dependence on the quark mass and the chiral condensate is introduced into the pseudoscalar solution

through the second (first-derivative) term in Eq. (30), while the scalar equation of motion does not have such a term. This difference should be attributed to distinct mass spectra and dissociation temperatures between the scalar and pseudoscalar mesons like the vector and axial-vector cases.

Here again, we shall trace the same procedures as those from Eq. (13) to Eq. (20). The potentials for the scalar and pseudoscalar fields in the picture of the Schrödinger equation are read from the equations of motion as

$$U_s(\xi) = \xi^2 + \frac{15}{4\xi^2} - \frac{f'}{2f}\left(2\xi + \frac{3}{\xi}\right) - \frac{(f')^2}{4f^2} + \frac{f''}{2f} - \left(\frac{\omega^2}{f^2} - \frac{k^2}{f}\right), \tag{31}$$

$$U_\pi(\xi) = \xi^2 + \frac{15}{4\xi^2} - \frac{f'}{2f}\left(2\xi + \frac{3}{\xi}\right) - \frac{(f')^2}{4f^2} + \frac{f''}{2f} - \left(\frac{\omega^2}{f^2} - \frac{k^2}{f}\right) - \frac{3}{\xi^2 f}. \tag{32}$$

Remarkably, the potential for the pseudoscalar field is independent of the background solution X_0 since all the terms depending on X_0 are put together into a form of the equation of motion (7). The difference between the scalar and pseudoscalar fields is only the last term in Eq. (32). We depict these potentials in Figs. 5 and 6. The results look very similar and turn monotonic around $t \simeq 0.12$.

Then we find that the behavior of the solutions in the near-horizon region is again given by $\phi_\pm$. In the opposite side of the UV limit we have two solutions for the scalar and pseudoscalar fields. That is,

$$s(\xi) = A_s\Phi_1'' + B_s\Phi_0'', \qquad \pi(\xi) = A_\pi\Phi_1 + B_\pi\Phi_0, \tag{33}$$

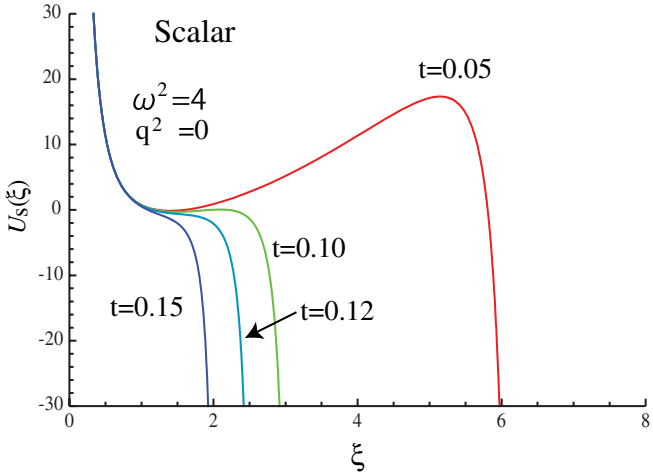

FIG. 5 (color online). Potential $U_s(\xi)$ for the scalar fields at dimensionless temperatures, $t = 0.05$, 0.10, 0.12, and 0.15 at $\omega^2 = 4$ and $q^2 = 0$. $\xi = \sqrt{c}z$, $t = T/\sqrt{c}$, and ω and q are given in the unit of $\sqrt{c}$.

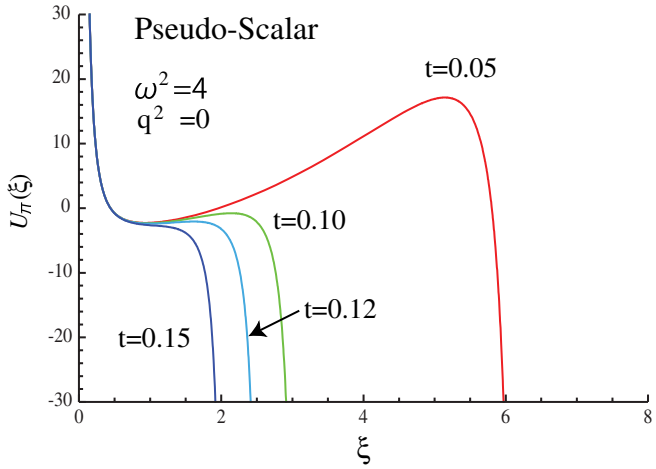

FIG. 6 (color online). Potential $U_\pi(\xi)$ for the pseudoscalar fields at dimensionless temperatures, $t = 0.05$, 0.10, and 0.15 at $\omega^2 = 4$ and $q^2 = 0$ with $\xi = \sqrt{c}z$. $\xi = \sqrt{c}z$, $t = T/\sqrt{c}$, and ω and q are given in the unit of $\sqrt{c}$.

where Φ_0 and Φ_1 are defined in Eq. (16) and Φ_0'' and Φ_1'' are the solutions of the equation of motion (29) with the boundary conditions; $\Phi_0''(\xi = \epsilon) = \epsilon$ and $\Phi_1''(\xi = \epsilon) = \epsilon^3$.

Here, let us note that, strictly speaking, the scalar field corresponding to the scalar source at the boundary is $s(\xi)/\xi$, and thus the boundary solutions behave asymptotically as 1 and ξ^2 like the other channels. Therefore the SPFs are characterized by the imaginary part of the complex coefficients B_s and B_π. To calculate the retarded Green's function we fix B_s and B_π requiring the in-falling boundary condition near the horizon.

We numerically calculate $\mathrm{Im}B_s$ and $\mathrm{Im}B_\pi$ and make plots as a function of ω at $q = 0$ in Figs. 7 and 8. Here, we present $\mathrm{Im}B_\pi$ divided by 10^3 since the normalization

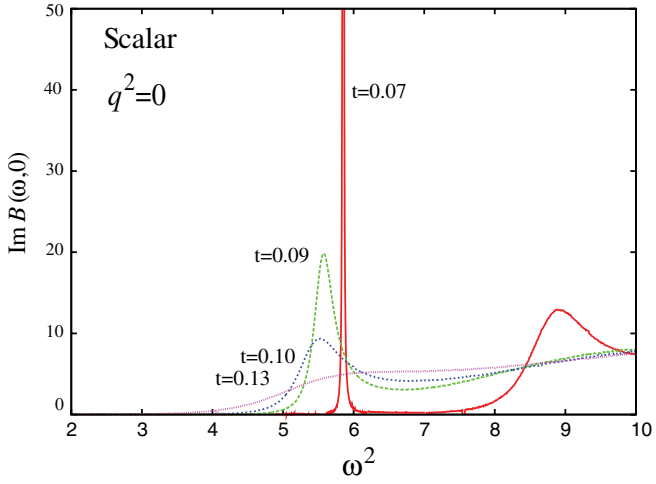

FIG. 7 (color online). Scalar spectral functions $\mathrm{Im}B(\omega, 0)$ for the temperatures, $t = 0.07$, 0.09, 0.10, and 0.13. $t = T/\sqrt{c}$, and ω and q are given in the unit of $\sqrt{c}$.

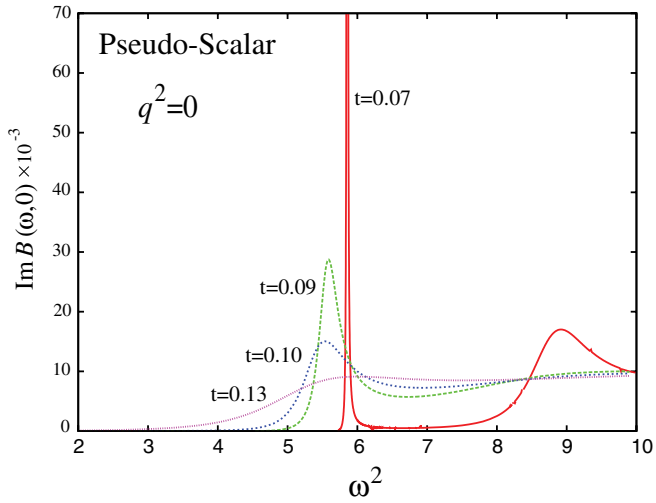

FIG. 8 (color online). Pseudoscalar spectral functions $\mathrm{Im}B(\omega,0)\times10^{-3}$ for the temperatures, $t=0.07$, 0.09, 0.10, and 0.13. $t=T/\sqrt{c}$, and ω and q are given in the unit of $\sqrt{c}$.

$A=1$ gives an irrelevant overall factor again. The lowest-lying peak at small temperature for the scalar and pseudoscalar channels is located at $\omega^2=5.85$. The model outputs for the meson masses are thus $m_{\chi_{c0}}\approx m_{\eta_c}=3.8$ GeV, which is not good as compared with $m_{\eta_c}=3.0$ GeV and $m_{\chi_{c0}}=3.4$ GeV. The scalar spectral peaks are located around $\omega^2=(4n+6)c$ with $n=0,1,2,\ldots$ for low temperatures, as is consistent with the results in Ref. [52]. Here, we see that the pseudoscalar spectral peaks are found at nearly the same positions as the scalar mesons.

The lowest-lying peaks are gradually collapsed and moving smaller as the temperature increases, while the excited peaks dissociate much earlier and shift more drastically. These spectral patterns are qualitatively similar to the vector and axial-vector cases. We can observe that the lowest-lying spectral peaks melt out around $t\simeq0.13$, i.e. $T=0.13\sqrt{c}=0.20$ GeV for the scalar and pseudoscalar channels both, which is slightly above the deconfinement temperature; $T\simeq1.05T_c$. If we take a closer look at the respective SPFs, we notice that the scalar meson melts only slightly earlier than the pseudoscalar meson. The difference is, however, hardly perceivable and we can say that the scalar and pseudoscalar channels are degenerate regardless of the chiral symmetry breaking.

V. MORE DISCUSSION ON THE VECTOR MESONS

We have seen that only the vector meson, i.e. J/ψ, survives above T_c (up to $T\simeq1.2T_c$ in our model), the axial-vector χ_{c1} suddenly disappears at $T=T_c$, and the scalar χ_{c0} and pseudoscalar η_c immediately melt around $T\simeq1.05T_c$. Therefore, it should be worth while taking a more serious look at the vector SPFs only. In this section we analyze the vector SPFs by deducing the relation between the mass shift Δm and the width broadening Γ with changing t. We also discuss the evolution of the SPFs at finite momentum q. Finally, we briefly mention on the dependence on the polarization direction.

A. Mass shift and width broadening

According to our previous work [29], a functional ansatz, $a\omega^b/[(\omega-\omega_0)^2+\Gamma^2]$ can fit the SPFs pretty well. In this way we can numerically read the peak position $\omega_0(t)$ (leading to the mass shift defined by $\Delta m(t)=\omega_0(0)-\omega_0(t)$) and the width $\Gamma(t)$ determined as a function of t.

In Fig. 9, we plot the mass shift squared $(\Delta m)^2$ and the width Γ associated with the lowest-lying peak in the vector and axial-vector SPFs. It is an intriguing finding from Fig. 9 that, even though the SPFs shown in Figs. 2 and 4 look similar at a glance, the qualitative behavior of the mass shift is completely different. In the case of the vector meson Δm^2 is saturated as t increases, while Γ continues growing. The relation between Δm and Γ has been investigated in the QCD sum rule [53], which is seemingly inconsistent with Fig. 9 but a careful consideration clarifies consistency [54]. In the previous work in Ref. [29] we proposed a definition for the dissociation temperature by means of the saturating behavior of Δm^2 around $t=0.14$. This working definition works for the vector meson, while the axial-vector peak keeps becoming lighter (i.e. larger Δm^2) and broader (i.e. larger Γ) and thus there is no saturation observed. It is an interesting question whether our prediction about the relation between Δm^2 and Γ in the axial-vector channel can be confirmed or not in other models such as the QCD sum rule.

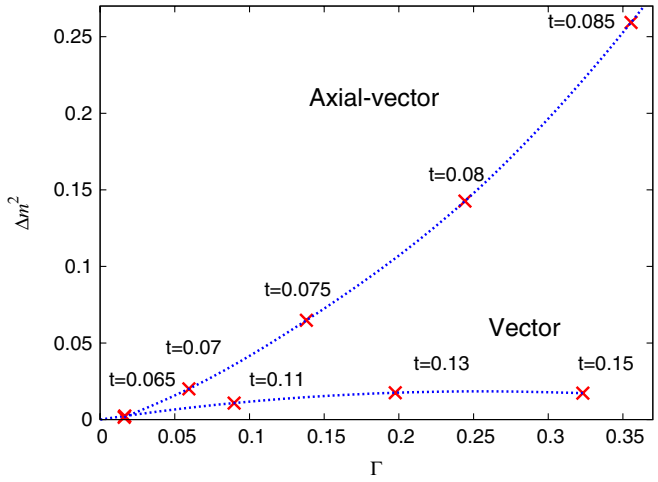

FIG. 9 (color online). Mass shift squared as a function of the width with changing temperatures. The dashed curve smoothly connects the calculated points at various temperatures for the vector and axial-vector channels.

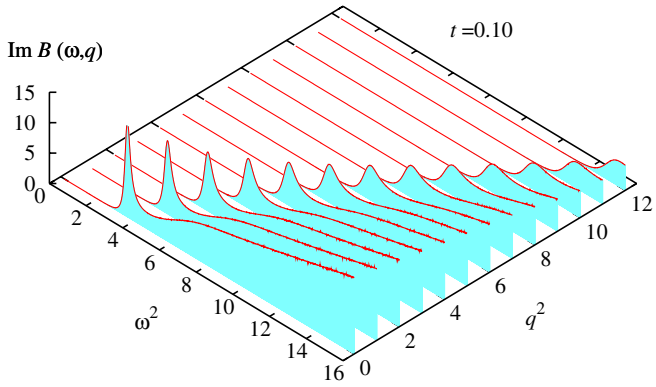

FIG. 10 (color online). Spectral functions $\mathrm{Im}B(\omega, q)$ as a function of ω and q for a fixed temperature $t = 0.10$, where ω, q, and t are all dimensionless in the unit of $\sqrt{c}$.

B. Finite momentum

In this subsection we briefly discuss the momentum dependence of the SPFs. There are several lattice QCD results on the J/ψ SPFs at finite momentum [55,56]. Although it is not clear whether the lattice simulation achieves accuracy enough to be reliable, the general tendency is that the spectral peaks are attenuated as q get larger.

Here, we present the results only for the vector channel because only J/ψ survives above T_c in the soft-wall model, which is our finding in this paper. We plot the numerical results in Fig. 10 for q^2 ranging from 0 to 12 with $t = 0.10$ fixed. We choose this temperature to make it easier to grasp the qualitative feature of the fairly prominent peaks in the SPFs, though we know that $t = 0.10$ is below T_c. The conclusion is, of course, unaltered even if we carry the analysis out on the case at $T > T_c$ as long as the peak remains.

It is apparent that the spectral peak is gradually collapsed as q increases. This result is quite nontrivial and peculiar to the nonperturbative regime since in the perturbative evaluation a larger q makes the spectral peak less sensitive to the medium effect [57]. It has been studied in Ref. [58] that, in the strongly correlated $N = 4$ super Yang-Mills theory, J/ψ melts at high q, or in a frame where J/ψ is at rest, it melts under the hot wind of quark-gluon plasma (QGP) matter. This conclusion has been confirmed in the top-down holographic QCD model later [59]. The discussions in Refs. [58,59] did not originate from the shape of the SPFs, however. Our present results add another confirmation of the hot screening scenario, and maybe the first evidence directly inferred from the shape of the SPFs.

C. Polarization dependence

We finally discuss the vector solution of the equation of motion (12). We can easily see that the equation of motion takes slightly different forms depending on whether the polarization is V_x or V_0. One may think that this difference should be interpreted as distinct behavior of the transverse and longitudinal modes in a medium. In fact, usually, if we see some vectorlike collective excitations with finite momentum q that is directed to q_3 for the moment, a linear combination of 0th and 3rd components describes the longitudinal mode, which becomes distinguishable from the transverse modes.

In this sense, it is surprising that Eq. (12) takes completely the same form regardless of the choice of $x = x_1$, x_2, or x_3, that is, Eq. (12) is insensitive to whether V_μ is parallel or perpendicular to q. This is a very strong statement. Usually, the transverse and longitudinal polarizations become degenerated only when $q = 0$ because the rotational symmetry is restored then [60]. (See also Ref. [61] for the hydrodynamic limit of the longitudinal mode.)

We point out that the above-mentioned statement can translate into the interpretation that there is no jet in the strong-coupling regime [62]. In our case the equation of motion and thus all the physical results are given as a function of q^2 only and V_x's are completely equivalent for $x = x_1$, x_2, and x_3. This means that the rotational symmetry of the system is not broken at all even though a finite momentum q is inserted. One can intuitively understand this as quick realization of the equipartition of inserted momentum over the system. Such a picture is very similar to the finding of Ref. [62] that no jet can exist in a strong-coupling $\mathcal{N} = 4$ supersymmetric Yang-Mills medium. Actually, if we assume the vector dominance, we can apply our results of the vector SPFs directly for the problem of the dilepton production, which may be an interesting direction regarding the future extension of our work.

VI. SUMMARY

In this paper we derived the SPFs of meson states in the vector, axial-vector, scalar, and pseudoscalar channels at finite temperature using the soft-wall AdS/QCD model. We pointed out that the SPFs in these channels have several qualitative features as follows:

(i) Only J/ψ survives above the deconfinement transition up to $T \simeq 1.2T_c$ and χ_{c1} completely melts at the transition. The scalar χ_{c0} and pseudoscalar η_c are almost degenerate in our model and melt soon above T_c.

(ii) In a deconfined state represented by the AdSBH metric, which is not energetically favored at $T < T_c$ in equilibrium but could exist as a meta-stable state for a wider range of T, the relation between the mass shift squared Δm^2 and the width Γ is characteristic to J/ψ and χ_{c1}. In the vector channel Δm^2 looks almost linearly proportional to Γ at small temperatures until it is saturated at the dissociation. In the axial-vector channel, in contrast, both Δm^2 and Γ keep growing up with increasing temperature.

(iii) The spectral peaks diminish at finite momentum, as is consistent with the scenario of the J/ψ suppression under a hot wind of QGP matter.

(iv) All the results on the vector and axial-vector-meson properties respect the rotational symmetry regardless of the presence of the momentum insertion. This should be interpreted as the equipartition of the momentum in a medium in the strong-coupling regime.

For more realistic studies to investigate the nonperturbative aspect of QCD, we need to construct a better model than the soft-wall QCD model that we adopted in this work. In the process of concrete computations, in fact, we realized that the conventional soft-wall model does not satisfy the requirement that the bifundamental scalar field should be $X_0 \sim M_q z + \Sigma z^3$ near the UV boundary ($z \sim 0$) but leads to a logarithmic correction $z^3 \log(z)$. The presence of $z^3 \log(z)$ in the solutions of the equation of motion brings huge uncertainty in evaluating the chiral condensate Σ numerically for a given quark mass M_q.

In addition to this problem of the asymptotic solution, there is another problem, that is, the conventional soft-wall model cannot describe the chiral phase transition. In reality what should be expected is that chiral symmetry is restored at the deconfinement transition simultaneously and then the vector and axial-vector channels become identical. In our case the quark mass is significantly heavy and breaks chiral symmetry badly, and thus we can consider that the lack of chiral restoration does not affect our results. Nevertheless, it is not clear *a priori* if not only M_q but also Σ have a substantial effect on the discrepancy between the vector and axial-vector mesons. To circumvent all these problems we will be able to use the modified soft-wall model [44,45] or the top-down approaches such as the D3/D7 and Sakai-Sugimoto models [63].

There are many directions in which the present work can be extended in the future. One example is the application to the dilepton production problem for which the vector SPF is the essential ingredient. We could maybe use more realistic holographic models mimicking the QCD equation of state [64]. It is also an interesting generalization to introduce not only the temperature effect but also the baryon density or the baryon chemical potential. Then, the Chern-Simons coupling mixes the vector and axial-vector mesons [65], which leads to an additional spectral broadening [66].

ACKNOWLEDGMENTS

We are grateful to Y. Hidaka, Y. Kim, and M. Stephanov for discussions. M. F. thanks H. Hata for useful advice. T. M. and M. M. thank N. Ogawa for technical support. K. F. is supported by Japanese MEXT Grant No. 20740134 and also supported in part by the Yukawa International Program for Quark Hadron Sciences. T. K. (Contract No. 21-951), T. M. (Contract No. 21-1226), and M. M. (Contract No. 21-173) are supported by Grand-in-Aid for the Japan Society for Promotion of Science (JSPS) Research..

[1] M. Gyulassy and L. McLerran, Nucl. Phys. **A750**, 30 (2005).
[2] E. V. Shuryak, Nucl. Phys. **A750**, 64 (2005).
[3] K. Adcox *et al.* (PHENIX Collaboration), Nucl. Phys. **A757**, 184 (2005); J. Adams *et al.* (STAR Collaboration), Nucl. Phys. **A757**, 102 (2005); B. B. Back *et al.*, Nucl. Phys. **A757**, 28 (2005); I. Arsene *et al.* (BRAHMS Collaboration), Nucl. Phys. **A757**, 1 (2005).
[4] J. M. Maldacena, Adv. Theor. Math. Phys. **2**, 231 (1998); Int. J. Theor. Phys. **38**, 1113 (1999).
[5] S. S. Gubser, I. R. Klebanov, and A. M. Polyakov, Phys. Lett. B **428**, 105 (1998).
[6] E. Witten, Adv. Theor. Math. Phys. **2**, 253 (1998); **2**, 505 (1998).
[7] G. Policastro, D. T. Son, and A. O. Starinets, Phys. Rev. Lett. **87**, 081601 (2001).
[8] A. Buchel and J. T. Liu, Phys. Rev. Lett. **93**, 090602 (2004).
[9] P. Kovtun, D. T. Son, and A. O. Starinets, Phys. Rev. Lett. **94**, 111601 (2005).
[10] J. I. Kapusta and T. Springer, Phys. Rev. D **78**, 066017 (2008).
[11] D. Teaney, Phys. Rev. C **68**, 034913 (2003).
[12] P. Romatschke and U. Romatschke, Phys. Rev. Lett. **99**, 172301 (2007).
[13] A. Hosoya and K. Kajantie, Nucl. Phys. **B250**, 666 (1985).
[14] P. Arnold, G. D. Moore, and L. G. Yaffe, J. High Energy Phys. 11 (2000) 001; 05 (2003) 051.
[15] G. Aarts and J. M. Martinez Resco, J. High Energy Phys. 04 (2002) 053.
[16] A. Nakamura and S. Sakai, Phys. Rev. Lett. **94**, 072305 (2005).
[17] H. B. Meyer, Phys. Rev. D **76**, 101701 (2007).
[18] M. Asakawa, T. Hatsuda, and Y. Nakahara, Prog. Part. Nucl. Phys. **46**, 459 (2001).
[19] T. Umeda, R. Katayama, O. Miyamura, and H. Matsufuru, Int. J. Mod. Phys. A **16**, 2215 (2001).
[20] M. Asakawa and T. Hatsuda, Phys. Rev. Lett. **92**, 012001 (2004).
[21] S. Datta, F. Karsch, P. Petreczky, and I. Wetzorke, Phys. Rev. D **69**, 094507 (2004).
[22] G. Aarts, C. R. Allton, R. Morrin, A. P. O. Cais, M. B. Oktay, M. J. Peardon, and J. I. Skullerud, Proc. Sci., LAT2006 (2006) 126 [arXiv:hep-lat/0610065].

[23] T. Umeda, Phys. Rev. D **75**, 094502 (2007).
[24] T. Matsui and H. Satz, Phys. Lett. B **178**, 416 (1986).
[25] F. Karsch, M. T. Mehr, and H. Satz, Z. Phys. C **37**, 617 (1988).
[26] W. Lucha, F. F. Schoberl, and D. Gromes, Phys. Rep. **200**, 127 (1991).
[27] C. Y. Wong, Phys. Rev. C **72**, 034906 (2005).
[28] A. Mocsy and P. Petreczky, Phys. Rev. D **77**, 014501 (2008); Phys. Rev. Lett. **99**, 211602 (2007).
[29] M. Fujita, K. Fukushima, T. Misumi, and M. Murata, Phys. Rev. D **80**, 035001 (2009).
[30] L. Da Rold and A. Pomarol, Nucl. Phys. **B721**, 79 (2005).
[31] A. Karch, E. Katz, D. T. Son, and M. A. Stephanov, Phys. Rev. D **74**, 015005 (2006).
[32] J. Erlich, E. Katz, D. T. Son, and M. A. Stephanov, Phys. Rev. Lett. **95**, 261602 (2005).
[33] K. Ghoroku, N. Maru, M. Tachibana, and M. Yahiro, Phys. Lett. B **633**, 602 (2006).
[34] A. Karch and E. Katz, J. High Energy Phys. 06 (2002) 043.
[35] D. Mateos, R. C. Myers, and R. M. Thomson, Phys. Rev. Lett. **97**, 091601 (2006); R. C. Myers, A. O. Starinets, and R. M. Thomson, J. High Energy Phys. 11 (2007) 091.
[36] J. Erdmenger, N. Evans, I. Kirsch, and E. Threlfall, Eur. Phys. J. A **35**, 81 (2008).
[37] K. Ghoroku and M. Yahiro, Phys. Rev. D **73**, 125010 (2006).
[38] Y. Kim, J. P. Lee, and S. H. Lee, Phys. Rev. D **75**, 114008 (2007).
[39] D. T. Son and A. O. Starinets, J. High Energy Phys. 09 (2002) 042.
[40] G. Policastro, D. T. Son, and A. O. Starinets, J. High Energy Phys. 09 (2002) 043.
[41] D. Teaney, Phys. Rev. D **74**, 045025 (2006).
[42] O. Andreev and V. I. Zakharov, Phys. Lett. B **645**, 437 (2007).
[43] C. P. Herzog, Phys. Rev. Lett. **98**, 091601 (2007).
[44] J. P. Shock, F. Wu, Y. L. Wu, and Z. F. Xie, J. High Energy Phys. 03 (2007) 064.
[45] T. Gherghetta, J. I. Kapusta, and T. M. Kelley, Phys. Rev. D **79**, 076003 (2009).
[46] R. Casero, E. Kiritsis, and A. Paredes, Nucl. Phys. **B787**, 98 (2007).
[47] U. Gürsoy and E. Kiritsis, J. High Energy Phys. 02 (2008) 032; U. Gürsoy, E. Kiritsis, and F. Nitti, J. High Energy Phys. 02 (2008) 019; U. Gürsoy, E. Kiritsis, L. Mazzanti, and F. Nitti, Phys. Rev. Lett. **101**, 181601 (2008); J. High Energy Phys. 05, (2009) 033; Nucl. Phys. **B820**, 148 (2009).
[48] T. D. Cohen and L. Y. Glozman, Phys. Rev. D **65**, 016006 (2001); Int. J. Mod. Phys. A **17**, 1327 (2002); Mod. Phys. Lett. A **21**, 1939 (2006).
[49] S. de Haro, S. N. Solodukhin, and K. Skenderis, Commun. Math. Phys. **217**, 595 (2001).
[50] K. Skenderis, Classical Quantum Gravity **19**, 5849 (2002).
[51] A. Karch, A. O'Bannon, and K. Skenderis, J. High Energy Phys. 04 (2006) 015.
[52] P. Colangelo, F. Giannuzzi, and S. Nicotri, Phys. Rev. D **80**, 094019 (2009); A. S. Miranda, C. A. B. Bayona, H. Boschi-Filho, and N. R. F. Braga, J. High Energy Phys. 11 (2009) 119.
[53] K. Morita and S. H. Lee, Phys. Rev. Lett. **100**, 022301 (2008); arXiv:0908.2856.
[54] K. Morita and S. H. Lee (private communications).
[55] S. Datta, F. Karsch, S. Wissel, P. Petreczky, and I. Wetzorke, arXiv:hep-lat/0409147.
[56] G. Aarts, C. Allton, J. Foley, S. Hands, and S. Kim, Proc. Sci., LAT2006 (2006) 134 [arXiv:hep-lat/0610061].
[57] Y. Hidaka, O. Morimatsu, and T. Nishikawa, Phys. Rev. D **67**, 056004 (2003).
[58] H. Liu, K. Rajagopal, and U. A. Wiedemann, Phys. Rev. Lett. **98**, 182301 (2007).
[59] T. Faulkner and H. Liu, Phys. Lett. B **673**, 161 (2009).
[60] P. K. Kovtun and A. O. Starinets, Phys. Rev. D **72**, 086009 (2005).
[61] K. Jo, Y. Kim, H. K. Lee, and S. J. Sin, J. High Energy Phys. 11 (2008) 040.
[62] Y. Hatta, E. Iancu, and A. H. Mueller, J. High Energy Phys. 05 (2008) 037.
[63] T. Sakai and S. Sugimoto, Prog. Theor. Phys. **113**, 843 (2005).
[64] S. S. Gubser and A. Nellore, Phys. Rev. D **78**, 086007 (2008).
[65] S. K. Domokos and J. A. Harvey, Phys. Rev. Lett. **99**, 141602 (2007).
[66] M. Harada and C. Sasaki, Phys. Rev. C **80**, 054912 (2009).